JCB Journal of Cell Biology

ARTICLE

Chromosome structural anomalies due to aberrant spindle forces exerted at gene editing sites in meiosis

Marion Manil-Ségalen[1], Małgorzata Łuksza[1], Joanne Kanaan[1], Véronique Marthiens[2], Simon I.R. Lane[3], Keith T. Jones[3], Marie-Emilie Terret[1], Renata Basto[2], and Marie-Hélène Verlhac[1]

Mouse female meiotic spindles assemble from acentriolar microtubule-organizing centers (aMTOCs) that fragment into discrete foci. These are further sorted and clustered to form spindle poles, thus providing balanced forces for faithful chromosome segregation. To assess the impact of aMTOC biogenesis on spindle assembly, we genetically induced their precocious fragmentation in mouse oocytes using conditional overexpression of Plk4, a master microtubule-organizing center regulator. Excessive microtubule nucleation from these fragmented aMTOCs accelerated spindle assembly dynamics. Prematurely formed spindles promoted the breakage of three different fragilized bivalents, generated by the presence of recombined Lox P sites. Reducing the density of microtubules significantly diminished the extent of chromosome breakage. Thus, improper spindle forces can lead to widely described yet unexplained chromosomal structural anomalies with disruptive consequences on the ability of the gamete to transmit an uncorrupted genome.

Introduction

The microtubule (MT) spindle enables equal segregation of chromosomes between daughter cells during mitosis and meiosis. Checkpoints monitor the attachment of each chromosome to the spindle apparatus to ensure that this process is faithful (Etemad and Kops, 2016; Touati and Wassmann, 2016). Even though numerical errors induced by defects in spindle assembly have been extensively studied in mitosis and meiosis, not much is known about the mechanisms or the origins of structural errors arising during M-phase (Brunet et al., 2003; Nagaoka et al., 2011; Kolano et al., 2012; Sacristan and Kops, 2015). However, a link between abnormal mitosis and DNA damage has been established (Ganem and Pellman, 2012). For example, prolonged mitosis is often related to DNA damage (Rieder and Palazzo, 1992; Rieder and Maiato, 2004). Merotelic attachments, in which one kinetochore of a chromosome is attached to both spindle poles, are common in tumor cells with extra centrosomes (Ganem et al., 2009). These attachment errors cause chromosome mis-segregation at mitotic exit (Cimini et al., 2001) and subsequent formation of micronuclei and chromothripsis in daughter cells (Cimini et al., 2001; Crasta et al., 2012; Zhang et al., 2015).

In the absence of canonical centrosomes, which are made from a pair of centrioles and pericentriolar material (PCM), meiotic spindles form with an important contribution from chromosome-mediated MT nucleation pathways. Thus MT assembly is enhanced in the vicinity of meiotic chromosomes (Heald et al., 1996; Dumont et al., 2007; Dumont and Desai, 2012; Bennabi et al., 2016). In mouse oocytes, PCM aggregates remain despite centriole loss, a feature that describes them as acentriolar MT-organizing centers (aMTOCs). It is unclear how aMTOCs assemble in the absence of centrioles, but they largely contribute to meiotic spindle assembly (Maro et al., 1985; Dumont et al., 2007; Schuh and Ellenberg, 2007). In fully grown prophase I–arrested oocytes, aMTOCs constitute typically one to three large foci (Luksza et al., 2013). At meiotic entry, these foci stretch around the nuclear envelope and fragment in a dynein- and MT-dependent manner (Luksza et al., 2013; Clift and Schuh, 2015). The importance of such timely reorganization of aMTOCs has not been addressed.

Plk4 is the master regulator of centriole duplication (Bettencourt-Dias et al., 2005; Habedanck et al., 2005) and is also essential for meiotic and mitotic acentriolar spindle assembly in oocytes and early mouse embryos by stimulating MT growth (Coelho et al., 2013; Bury et al., 2017). In the present study, we took advantage of the role of Plk4 to perturb aMTOC organization in oocytes (Luksza et al., 2013). Transgenic overexpression of Plk4 (Marthiens et al., 2013) in oocytes during their growth phase in the ovary led to precocious aMTOC fragmentation before nuclear envelope breakdown (NEBD). It also led to earlier spindle bipolarization associated with greater MT nucleation.

[1]Collège de France, Centre for Interdisciplinary Research in Biology, UMR CNRS 7241/INSERM-U1050, Paris, France; [2]Institut Curie, Paris Sciences et Lettres Research University, Centre National de la Recherche Scientifique, UMR144, Biology of Centrosomes and Genetic Instability Laboratory, Paris, France; [3]Biological Science, Faculty of Natural and Environmental Sciences, University of Southampton, Southampton, UK.

Correspondence to Marie-Hélène Verlhac: marie-helene.verlhac@college-de-france.fr; S.I.R. Lane's present address is Institute for Life Sciences and Faculty of Chemistry, University of Southampton, Southampton, UK.

After NEBD, oocytes completed meiosis I. However, one bivalent broke into two pieces, consistent with breaks occurring near the recombined Lox P sites present in the genome of three different mouse lines. Crucially, a decrease in MT density significantly diminished the efficiency of bivalent breakage. Altogether, our work suggests that increasing MT density and probably forces exerted on fragilized chromosomes can lead to bivalent breakage during meiosis I, as shown here for three different chromosomes. This in turn leads to mis-segregation of chromosome fragments. Chromosome rearrangements and fragment losses are relatively frequent in human embryos and lead to severe pathologies. This is the case for intellectual disability syndromes such as Wolf–Hirschhorn caused by a 4p deletion (Wieczorek et al., 2000), the 9p deletion (Okten et al., 2009), or the 6q terminal deletion (Striano et al., 2006). We hypothesize that our work may identify one mechanism by which structural chromosome anomalies can arise during meiosis.

Results

Plk4 overexpression in growing oocytes causes premature aMTOC fragmentation

As previously published (Bury et al., 2017), we confirmed that Plk4 is present in mouse oocytes. For this, we labeled endogenous Plk4 by immunofluorescence in control oocytes blocked in prophase I of meiosis (Fig. 1 A, bottom left). By costaining with the PCM component pericentrin (Fig. 1 A, top left), we showed that Plk4 localizes to aMTOC, arguing that it is not a limiting factor for centriole assembly in oocytes.

To test the importance of aMTOC organization on spindle assembly (Bennabi et al., 2016), we took advantage of the role of Plk4 (Bury et al., 2017) to try and perturb them in oocytes using a novel approach. Conditional Plk4 overexpression in oocytes was achieved by crossing a line expressing the Cre-recombinase under the ZP3 promoter with a line containing a random insertion of a chicken β-actin promoter (CAG) fused to a floxed stop-codon and to mCherry-Plk4 (Fig. S3 A, referred to as Plk4 OE; Marthiens et al., 2013). The ZP3 promoter is active after birth, after homologous chromosomes have recombined and formed chiasmata, and only during oocyte growth (Lewandoski et al., 1997). In this way, we obtained excision of the stop-codon and expression of the m-Cherry-Plk4 transgenic construct exclusively in oocytes during their growth period at puberty.

In both Plk4 OE prophase I–arrested oocytes (from $Plk4^{flox/wt}$; Cre^{+} female mice) and control oocytes (coming either from $Plk4^{flox/wt}$; Cre^{-} or $Plk4^{wt/wt}$; Cre^{+} female mice), Plk4 was detected on aMTOCs (Fig. 1 A, bottom). However, Plk4 OE oocytes displayed modified aMTOC characteristics with numerous small foci in the vicinity of the nucleus (Fig. 1 A, right). In Plk4 OE oocytes, the amount of Plk4 at aMTOCs was more than six times higher than in controls (Fig. 1 B), while the amount of pericentrin at aMTOCs remained unchanged (Fig. 1 C). Because of the relative size of the oocyte and the aMTOCs, the local aMTOC signal corresponds to only 0.1% of the signal in the entire oocyte. It is thus not so surprising that no detectable increase in the total amount of either pericentrin or Plk4 was observed in whole Plk4 OE oocytes compared with controls (Fig. S1, A and B). These data argue that exogenous Plk4 preferentially accumulates on aMTOCs and is present there in large excess.

To describe the changes in the organization of aMTOCs, we performed 3D quantitative analysis of competent, fully grown Plk4 OE oocytes in prophase I (Fig. 1, D and E). The number and the cumulated surfaces of all aMTOCs were both significantly higher in Plk4 OE compared with controls. These observations suggested that aMTOCs were more fragmented in Plk4 OE oocytes.

aMTOC fragmentation occurs at the end of the prophase I block

We used 3D structured illumination microscopy (3D-SIM) to look more closely at the detailed morphology of PCM in prophase I–arrested Plk4 OE oocytes, as has been done in centriolar cells (Fu and Glover, 2012; Lawo et al., 2012; Mennella et al., 2012; Sonnen et al., 2012). In controls, oocytes display one major aMTOC, harboring a globular shape with the pericentrin matrix displaying multiple cavities filled with Plk4 (Luksza et al., 2013). In contrast, fully-grown Plk4 OE oocytes, competent to resume meiosis I, contained multiple aMTOCs that assembled into thread-like structures when running parallel to the nuclear envelope (Fig. S1 C, right). The pericentrin internal cavities were no longer detected in these long thread-like structures, indicating a dramatic change in PCM organization.

The superresolution microscopy data and the absence of increase in pericentrin labeling, together with the 3D quantifications of aMTOC organization, argue for a premature fragmentation of the PCM in Plk4 OE oocytes (Fig. S1 D). This fragmentation occurs at the end of oocyte growth, in prophase I, as incompetent Plk4 OE oocytes present only one globular pericentrin matrix, filled with Plk4, as in controls (Fig. S1, C [left] and D; Luksza et al., 2013). Thus, even if induced early on during the growth phase, Plk4 overexpression results in major changes in the organization of aMTOCs only at the end of the prophase I block, once the oocyte reaches competence to resume meiosis I.

Overexpression of Plk4 during the growth phase of the oocyte is needed for aMTOC fragmentation

The fragmentation of aMTOCs occurred at the end of the oocyte growth phase; thus, we tested whether a similar phenotype could be reproduced by directly injecting the cRNA encoding for mCherry-Plk4 into fully grown oocytes in prophase I (Fig. 2 A). When the mCherry-Plk4 cRNA is injected, much higher levels of Plk4 are reached than with Plk4 OE, both globally and associated with aMTOCs (Fig. 2, B–D). In the case of the cRNA, the total number of aMTOCs per oocyte was higher than in controls but was comparable to the number observed in the transgenic line overexpressing Plk4 (Fig. 2, B and E). However, instead of several aMTOCs presenting widths ranging from 1 to 5 μm^2 as in Plk4 OE oocytes (Fig. 2 F), in each injected oocyte we detected one large aMTOC and multiple tiny foci of mCherry-Plk4 (smaller than 1 μm^2; compare left vs. right panels in Fig. 2 B and see size quantification in Fig. 2 F). Although we do not know how these very small aMTOCs are generated, the large aMTOC is the dominant site for MT nucleation in these oocytes (Fig. 2 G, left). This is strikingly different from what can be observed in the Plk4 OE

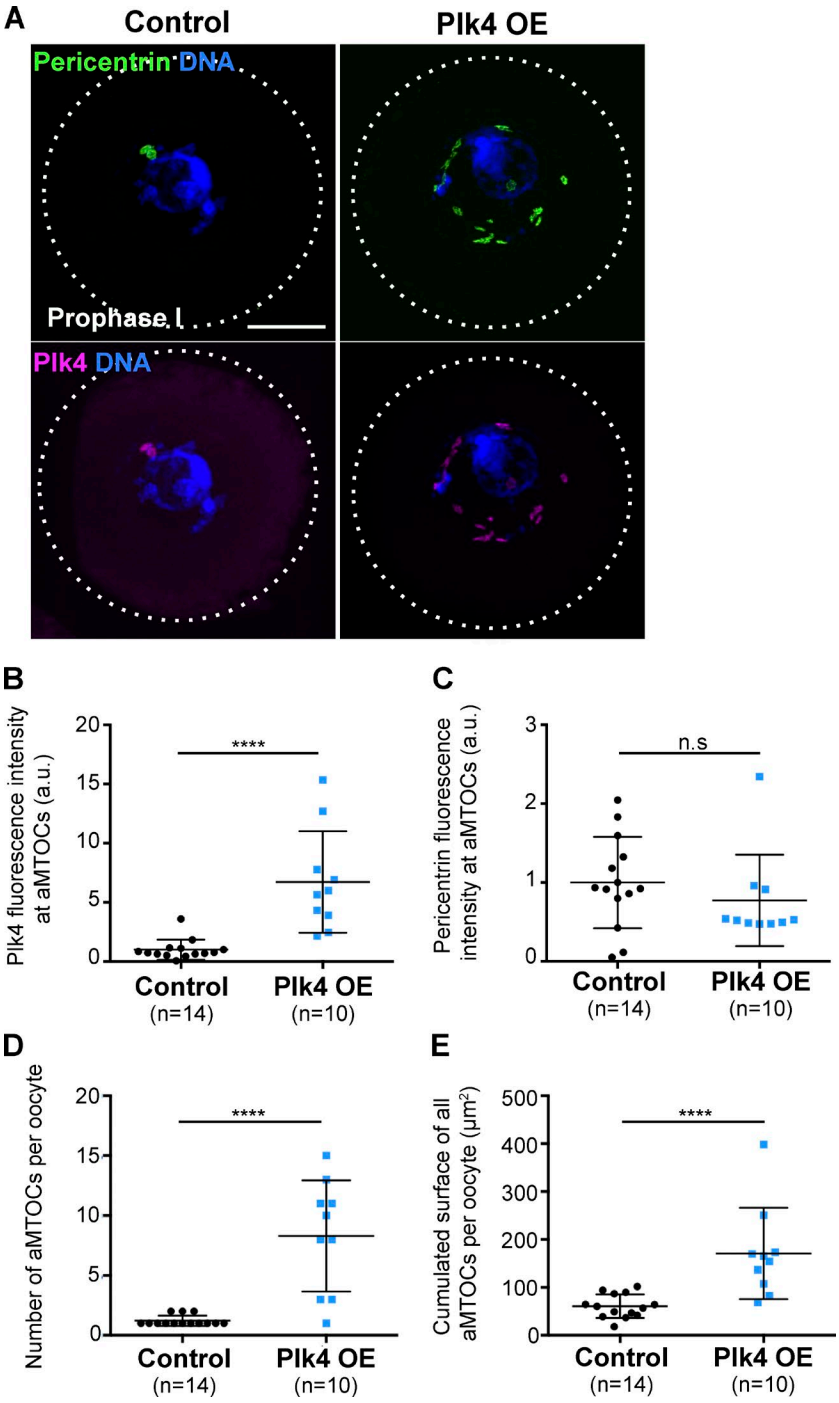

Figure 1. **Plk4 OE induces aMTOC precocious fragmentation. (A)** Immunofluorescent costaining of Plk4 (pink) and pericentrin (green) in control (left) and Plk4 OE (right) oocytes observed in prophase I. Scale bar is 10 µm. **(B)** Measure of Plk4 fluorescence intensity exclusively at nucleus associated aMTOCs from control (black dots) and Plk4 OE oocytes (blue squares) as observed in A; arbitrary units; ****, $P < 0.0001$. **(C)** Measure of pericentrin fluorescence intensity exclusively at nucleus associated aMTOCs from control (black dots) and Plk4 OE (blue squares) oocytes as observed in A; arbitrary units, $P = 0.2125$. **(D and E)** 3D quantitative analysis of aMTOCs number per oocyte **(D)** and their cumulated external surface per oocyte **(E)** in control (black dots) and Plk4 OE (blue squares) oocytes in prophase I as observed in A. ****, $P < 0.0001$ for number and surfaces. In B–E, statistical tests used are two-tailed Mann–Whitney, and *n* corresponds to the number of oocytes. Error bars correspond to SD.

transgenic prophase I oocytes, where all fragments of aMTOCs show significant MT nucleation (Fig. 2 G, right). Altogether, our results suggest that Plk4 overexpression during the growth phase of oocytes (via transgenic Plk4 OE), but not when limited to the competent/fully-grown stage (via cRNA injection), leads to premature fragmentation of aMTOCs into smaller functional units able to promote significant MT nucleation.

Fragmented aMTOCs have increased MT-nucleating capacity

To test the impact of precocious aMTOC fragmentation, oocytes were then allowed to resume meiosis, and local MT density was observed around the condensing chromosomes at the time of NEBD as done previously (Breuer et al., 2010). The intensity of EB3-GFP fluorescence in the vicinity of chromosomes was significantly higher (1.4×) in Plk4 OE oocytes, indicating that they contained more MT than controls (Fig. 3, A and B). Importantly, the increase in EB3-GFP intensity at NEBD correlated with the number of aMTOCs observed in prophase I (Fig. 3 C). However, such an increase in MT density at NEBD was not observed after overexpression of mCherry-Plk4 via cRNA injection into fully grown oocytes (Fig. 2 H), despite higher levels of overexpression reached by this approach (Fig. 2, C and D). This result suggests that the extent of aMTOCs fragmentation in prophase I impacts on the MT density at meiosis resumption.

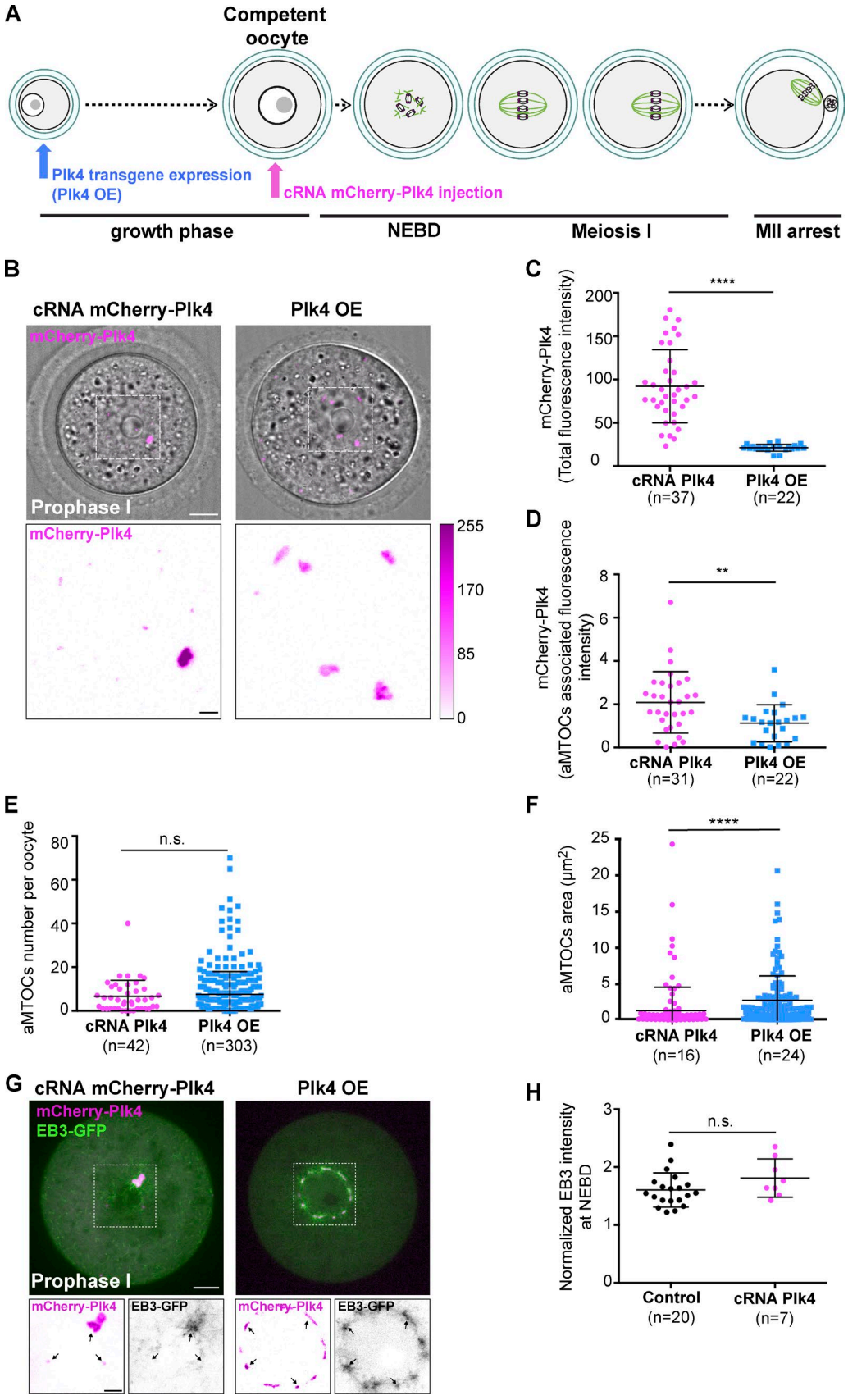

Figure 2. **Overexpression of Plk4 during oocyte growth induces aMTOC fragmentation. (A)** Schematic of the two methods for achieving mCherry-Plk4 OE in mouse oocytes: by either a transgenic approach allowing Plk4 OE at the beginning of the growth phase (in blue) or mCherry-Plk4 cRNA injection allowing Plk4 OE after the growth phase (in pink). mCherry-Plk4 cRNA was injected into competent/fully grown control oocytes and expressed 3 h before live imaging.

To estimate the consequences of an increased MT density at NEBD, we followed the formation of meiotic spindles in live EB3-GFP–injected oocytes (Fig. 3 D and Video 1). In control oocytes, the entire meiosis I lasts ∼9 h from NEBD until polar body extrusion (PBE). At early stages of meiosis resumption after NEBD, the newly assembled mass of MT self-organizes into a bipolar array ∼3–4 h after NEBD (Dumont et al., 2007; Schuh and Ellenberg, 2007). As expected from previous work (Dumont et al., 2007; Kolano et al., 2012), increased density of MT observed in Plk4 OE oocytes resulted in earlier spindle elongation and bipolar axis formation (on average 45 min earlier in Plk4 OE oocytes compared with controls; Fig. 3, D and E). This result was confirmed on fixed samples observed 4 h after NEBD and analyzed by immunofluorescence (Fig. S2, A and B). More oocytes (61.4% vs. 26.1%) contained a robust bipolar spindle in Plk4 OE oocytes compared with controls at 4 h after NEBD (Fig. S2 B). Thus, in Plk4 OE oocytes, meiotic spindle bipolarity is established earlier than in controls.

Plk4 OE oocytes are endowed with chromosome breakage

We then analyzed the consequences of premature increased density of MT early on during meiosis I. Unexpectedly, Plk4 OE oocytes frequently contained 21 individual chromosome fragments, instead of the normal 20 bivalent complement of mouse. Remarkably, we observed the appearance in live cells of a round chromosome, smaller than all others, that oscillated back and forth across the metaphase plate, suggesting it was not correctly bi-oriented (Fig. 4 A, black arrows; and Video 2). Indeed, this small DNA fragment had only one pair of kinetochores positive for Mad2-YFP (Fig. 4 A, right inset). We wanted to better characterize this breakage event, which has never been described previously in the first meiotic division without prior treatment with a DNA-damaging agent (Collins et al., 2015; Marangos et al., 2015; Lane et al., 2017). Therefore, oocytes were fixed at NEBD + 6h00, centromeres were labeled with CREST, and 3D reconstruction was used to count the number of bivalents in oocytes derived from two independent insertions of the same Plk4 transgene (transgenic lines A and B; see Materials and methods, Fig. S3 C, and Videos 3, 4, and 5). In transgenic line A, we observed the breakage of one bivalent as depicted in Fig. 4 A: one large and one small fragment, both of which harboring a pair of centromeres labeled with CREST (Fig. 4 B, upper; and Video 4, compare with Video 3). The pattern of breakage was very reproducible within this line (Fig. 4 C showing various examples artificially highlighted in blue). In line B, we also observed the breakage of a single bivalent, but different from line A, generating a fragment of DNA lacking CREST signal (Fig. 4, D and E; and Video 5) and much smaller than any fragment detected in oocytes from line A (Fig. 4 F). Without any centromere and thus devoid of the ability to assemble a kinetochore, this smaller fragment was not retained in the meiotic spindle (Fig. 4 D, left, and other examples of the small fragment artificially highlighted in green in Fig. 4 E). The frequency at which we could observe chromosome breakage in the two lines differed: it was more frequent in line A (27.0%) than in line B (10.2%; Fig. 4 G and summarized in Fig. S3 C). Differences in the rate of chromosome breakage between the two strains were not a result of different overexpression levels of Plk4, as no difference in mCherry-Plk4 expression was found at aMTOCs between the two lines (Fig. S4, A and B).

Because the breakage occurred only on one bivalent, in a specific manner for both transgenic lines, we hypothesized that it took place at the insertion site of the mCherry-Plk4 transgene—this being the only major difference between the two lines. The site of insertion was sequenced for both lines. In line A, it was found to be close to the centromeric region of chromosome 9, theoretically generating a small 45-Mb DNA fragment if the cut site occurs in the region of the transgene. In line B, it was close to the telomeric region of chromosome 12, which would generate a very small 15-Mb acentric DNA fragment if the cut occurs in the region of the transgene (Figs. 4 H and S3 C). These sites of insertion are fully consistent with the fragments observed in both lines: two fragments containing centromeres for line A (Fig. 4 B), and a smaller acentric fragment for line B (Fig. 4 D).

To support the sequencing data, we performed FISH experiments on oocytes from line A. The chromosome fragments corresponded to the genome location of transgene insertion, as 100% of the observed broken chromosomes were labeled with a FISH probe for chromosome 9 (Fig. 4 I). Chromosome breaks were never observed in oocytes coming from $Plk4^{flox/wt}$; Cre^{-} mice or $Plk4^{wt/wt}$; Cre^{+} female mice (our negative controls that do not overexpress Plk4) or in the mCherry-Plk4 cRNA-injected oocytes (Fig. S2 C). Furthermore, we know that recombination and repair of the mCherry-Plk4 transgene did happen in all Plk4 OE oocytes from both lines, since 100% of them were positive for mCherry-Plk4. Therefore, it can be excluded that the break took place early on during oocyte growth. Our data strongly support

Plk4 OE oocytes were imaged directly upon isolation. Gray, chromosome; pink, kinetochores; green, MTs. MII, metaphase II. **(B)** Upper panels correspond to the merge of transmitted light images with the mCherry-Plk4 fluorescent image in cRNA-injected (left) versus transgenic Plk4 OE (right) oocytes observed in prophase I (mCherry-Plk4, magenta). The white dotted square highlights the nuclear area, and the mCherry-Plk4 signal from this region is displayed on the lower panels. The signal intensity lookup table is depicted on the right side. Scale bar is 10 µm (upper panels) or 2 µm (lower panels). **(C)** Total levels of mCherry-Plk4 expression measured as absolute signal intensity from oocytes in prophase I, either cRNA-injected (purple dots) or from Plk4 OE (blue squares) as observed in B; ****, $P < 0.0001$ (two tailed *t* test with Welch correction). **(D)** aMTOC-associated levels of mCherry-Plk4 overexpression measured as absolute signal intensity from oocytes in prophase I, either cRNA-injected (purple dots) or from Plk4 OE (blue squares); **, $P = 0.0046$. **(E)** 2D quantitative analysis of aMTOC number in oocytes injected with mCherry-Plk4 cRNA (purple dots) and from Plk4 OE (blue squares); $P = 0.8752$. **(F)** 2D quantitative analysis of aMTOC area in oocytes injected with mCherry-Plk4 cRNA (purple dots) and from Plk4 OE (blue squares); ****, $P < 0.0001$. **(G)** EB3-GFP (green) is presented to visualize MT organization in cRNA-injected (left) versus Plk4 OE (right) prophase I oocytes. The EB3-GFP signal (green) is merged with the mCherry-Plk4 signal (magenta). The white dotted boxes highlight the nuclear regions. Insets are higher magnifications of signals from nuclear regions. In insets, the EB3-GFP signal appears black while mCherry-Plk4 appears magenta. The black arrows point toward aMTOCs. Scale bars are 10 µm (upper panels) and 5 µm (lower insets). **(H)** Normalized signal intensity of the EB3-GFP signal around chromosomes in oocytes observed at NEBD from controls (black dots) or injected with mCherry-Plk4 cRNA (pink dots). $P = 0.1358$. In D–F and H, the statistical tests used were two-tailed Mann–Whitney. Error bars correspond to SD. In all graphs, *n* is the number of oocytes.

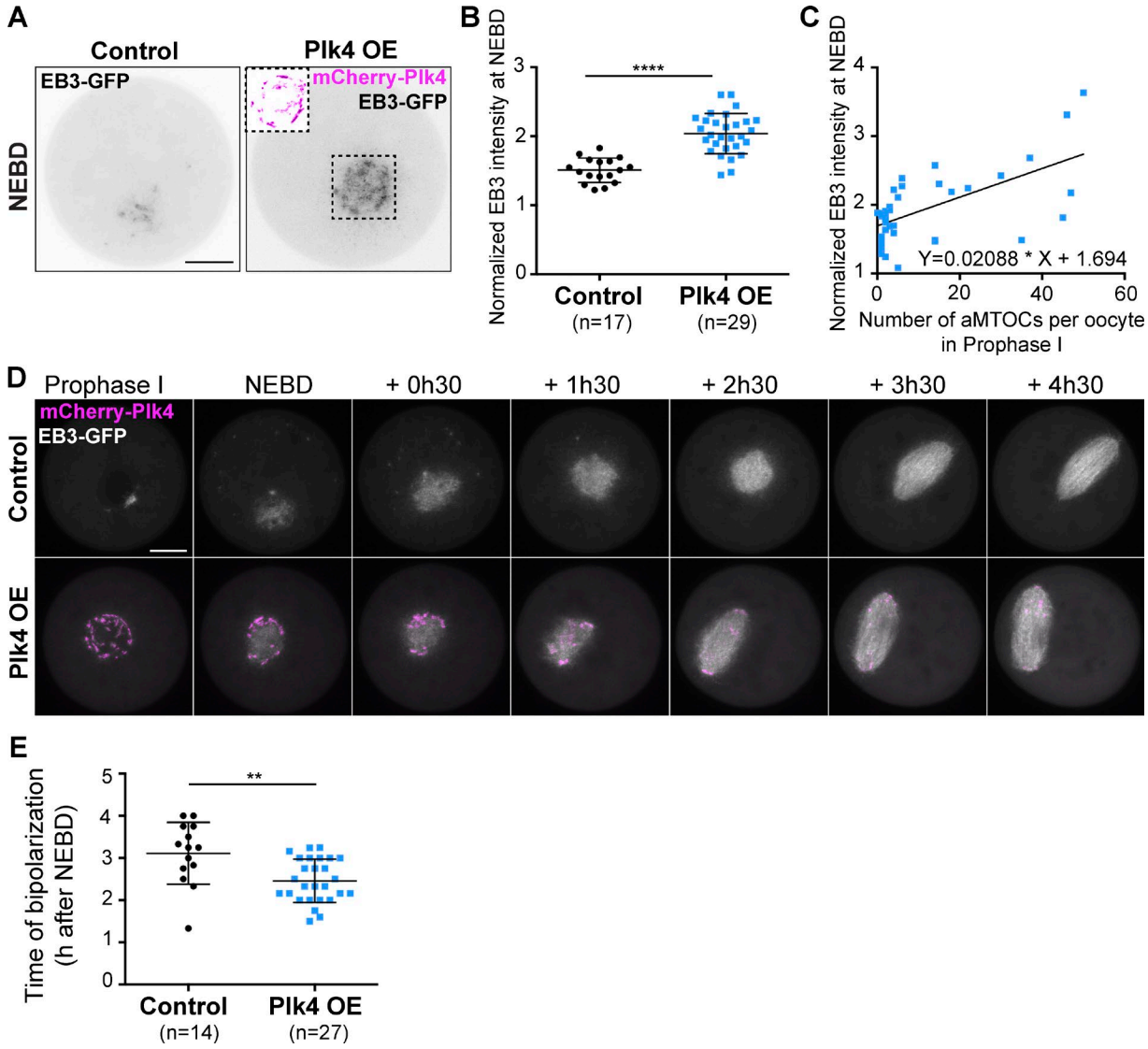

Figure 3. **Fragmented aMTOCs have increased MT-nucleating activity at NEBD. (A)** EB3-GFP expression in control (left) and Plk4 OE (right) oocytes observed at NEBD. The black dotted square shows the mCherry-Plk4 labeling (pink) that surrounds early spindle MT, visible only in Plk4 OE oocytes. EB3-GFP appears in gray levels. Scale bar is 10 µm. **(B)** Normalized signal intensity of EB3-GFP around chromosomes in control (black dots) and Plk4 OE (blue squares) oocytes observed at NEBD. The signal was measured in a Ø20-µm region around the chromosomes; total signal intensity was measured in a Ø70-µm region covering the whole oocyte. Normalized signal intensity is the ratio of local/total intensity measured for individual oocytes; ****, P < 0.0001. **(C)** Correlation between the number of aMTOCs in prophase I and normalized fluorescence intensity of EB3-GFP at NEBD (n = 37). Normalized EB3-GFP fluorescence intensity measured at NEBD is plotted against the number of aMTOCs per oocyte in prophase I. **(D)** Early steps of spindle formation in control versus Plk4 OE oocytes expressing EB3-GFP. Oocytes were followed from prophase I exit until spindle bipolarization. EB3-GFP appears white and mCherry-Plk4 pink. Scale bar is 15 µm. Timing (expressed in hours and minutes) is relative to NEBD. **(E)** Timing of spindle bipolarization observed in living oocytes expressing EB3-GFP as presented in D; **, P = 0.0076. For B and E, the statistical tests used are two-tailed t test with Welch correction, and n corresponds to the number of oocytes. Error bars correspond to SD.

the view that the chromosome breakage occurs at or near the site of the recombined transgenic insertion at late stages of oocyte growth or even later during the division (Fig. 4 J).

Chromosome breakage can occur at any Cre-recombined Lox P site provided aMTOCs are fragmented

We then tested whether the creation of another fragile site, different from the transgenic Plk4 insertion, could also be associated with breakage of one bivalent. For this, we crossed Plk4 line $A^{flox/wt}$; Cre^{+} mice with $MyoX^{flox/wt}$; Cre^{-} mice. The $MyoX^{flox/wt}$; Cre^{-} line has been constructed by insertion of two Lox P sites between exon 26 and exon 30 of the myosin X endogenous locus in chromosome 15 (Fig. S3 B). These mice are fertile and display no obvious phenotype in their oocytes (not depicted and Fig. 5, lower panels). Oocytes coming from the Plk4 line $A^{flox/wt}$; Cre^{+}; $MyoX^{flox/wt}$ females were fixed at NEBD + 6h00 (as done in Fig. 4, B and D), and their chromosomes were counted. 12.5% of these oocytes displayed a broken bivalent resembling the one observed in Plk4 line A (Fig. 5 A, upper panels, blue arrows), while 15.6% presented a new type of break: a large piece of DNA, with no

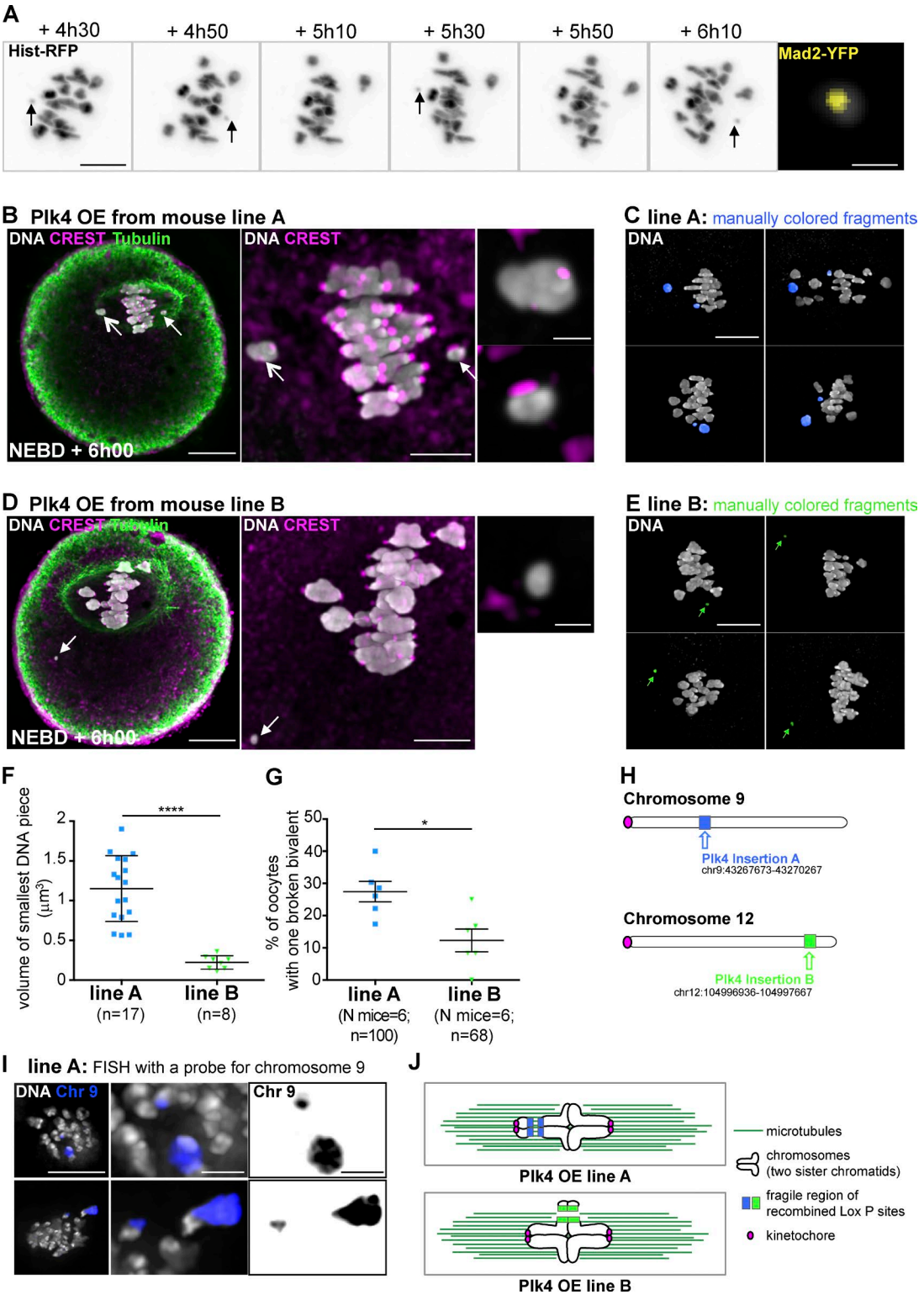

Figure 4. **Evidence for chromosome breakage in two transgenic lines overexpressing Plk4. (A)** Time-lapse images of chromosomes labeled with histone-RFP followed in Plk4 OE (line A) during meiosis I. Black arrows point at the smallest chromosome fragment moving back and forth on the metaphase plate. Chromosomes appear in gray levels. Timing (expressed in hours and minutes) is relative to NEBD. Scale bar is 10 µm. The right panel shows the smallest DNA fragment (gray) at a higher magnification harboring a Mad2-YFP signal (yellow) at NEBD + 6h10. Scale bar is 1 µm. **(B and D)** Immunofluorescent costaining of DNA (white), CREST (pink), and Tubulin (green) in Plk4 OE line A (B) and line B (D) oocytes observed at NEBD + 6h00. White arrows point at the chromosome pieces. Higher magnification of DNA pieces is shown in the right panels: the upper right panel corresponds to the largest one and the lower right panel to the smallest one. Scale bar is 20 µm in the left panels, 5 µm in the middle panels, and 1 µm in the right panels. **(C and E)** Examples of fixed oocytes with broken bivalents in line A (C) and line B (E) observed at NEBD + 6h00. Broken bivalents have been artificially colored in blue for line A (C) and in green for line B (E). Scale bar is 5 µm. **(F)** Quantitative analysis of the volume of the smallest chromosome fragment in oocytes from Plk4 OE lines A and B observed at NEBD +

centromere (Fig. 5 A, lower panels, orange arrow; and Video 6). We did not observe oocytes presenting the two types of break simultaneously. Their frequency might be too low, and we did not look at enough oocytes coming from this double cross (Fig. 5 B). The volume of the new acentric fragment was significantly larger than the smallest DNA piece observed in both line A and line B (Fig. 5, C and D). We interpret this new type of break as a breakage at the MyoX locus on chromosome 15 (Fig. 5, E and F), since it is consistent with the larger size of the acentric fragment as well as with the potential chiasma location on this chromosome (Morgan et al., 2017). Acentric fragments of chromosomes are not retained in the spindle (see Fig. 4 D). Remarkably, we observed 2/3 of oocytes with the large acentric fragment close to the metaphase plate (Fig. 5 D, left), while 1/3 was away from the spindle (Fig. 5 D, right). This observation could indicate that the fragile bivalent is cut into two pieces while meiosis I progresses. Importantly, no chromosome break was observed in control oocytes from Plk4 line $A^{flox/wt}$; Cre^{-}; $MyoX^{flox/wt}$ or Plk4 line $A^{wt/wt}$; Cre^{+}; $MyoX^{flox/wt}$ females (Fig. 5 A, lower panels). This indicates that the break occurs only when two conditions are met: Plk4 overexpression associated with aMTOC fragmentation and recombined Lox P sites. These data argue that sites breaking under tension can be created in the genome, outside the Plk4 insertion.

Extent of bivalent breakage correlates with the extent of aMTOCs spreading and MT density

Plk4 OE oocytes have fragmented aMTOCS, nucleate more MTs and thus present an accelerated spindle formation. All this could cause changes in forces applied on chromosomes during meiosis I and favor chromosome breakage. We went on to characterize further the relationship between spindle dynamics and the generation of broken bivalents.

First, we compared line A and line B. As mentioned previously, more chromosome fragments are observed in line A than in line B (Fig. S3 C). Consistently, we observed that the extent of aMTOC fragmentation in prophase I was higher in line A than in line B (Fig. 6 A), despite them having the same level of overexpression at the end of oocyte growth (Fig. S4, A and B). Kinetics of synthesis and/or recruitment of Plk4 might be different between lines during the growth phase of oocytes, potentially impacting aMTOC biogenesis.

We then counted oocytes presenting a broken chromosome at different time points in meiosis I (in Plk4 OE from line A). At 4h00 after NEBD, we observed only 5.4% of oocytes with a broken bivalent, compared with 27.0% at 6h00 after NEBD (Fig. 6 B). At this stage, oocytes already have individualized chromosomes easier to count than at 6h00 after NEBD, when they are aligned on the metaphase plate (Fig. S2 A and Video 7). The percentage of oocytes that presented a broken chromosome increased significantly as meiosis I progresses, as the spindle assembles and k-fibers are formed (Dumont et al., 2007; Schuh and Ellenberg, 2007; Breuer et al., 2010; Bennabi et al., 2016).

Because MT density is increased in Plk4 OE, maybe owing to the increase in the surface of nucleation from fragmented aMTOCs (Figs. 1 E and 2 B), we tested whether lowering MT density would impact the extent of bivalent breakage. To achieve this, Plk4 OE oocytes from line A were incubated with very low doses of nocodazole (ranging from 50 to 100 nM). As previously shown, such doses impact on spindle MT density (Fig. 6, C and D). The treatment with 50 nM nocodazole had a tendency to reduce the percentage of breakage events normally observed 6 h after NEBD (from 23.3% in controls down to 14.0% with 50 nM nocodazole, P = 0.172) while higher doses (100 nM) significantly reduced breakage events (from 23.3% in controls down to 6.1% with 100 nM nocodazole, P = 0.0068; Fig. 6 E and Video 8). This suggested that bivalent breakage was a consequence of increased MT density. Altogether, our results argue for a positive correlation between aMTOC fragmentation, earlier spindle bipolarization due to increased density of MTs, and DNA breakage.

Plk4 OE oocytes progress less efficiently throughout meiosis I

We then tested if the presence of a broken bivalent would affect cell cycle progression of Plk4 OE oocytes. We live-imaged Plk4 OE oocytes throughout meiosis I. These oocytes were delayed by almost 2 h in PBE timing compared with controls (Plk4 OE, 10h50 ± 2h00; controls, 9h05 ± 1h36; Fig. 7 A). The delay was most probably due to spindle assembly checkpoint (SAC) activation, since it could be rescued using the Mps1 inhibitor, reversine, as previously described (Hached et al., 2011; Kolano et al., 2012). In the presence of reversine, Plk4 OE underwent PBE with kinetics and efficiency comparable to controls (Fig. 7 A). However, the maintenance of an active SAC was not due to the presence of a broken bivalent. Indeed, by following the chromosomes using histone-GFP in live cells, we could detect the presence of a small broken fragment, yet anaphase I occurred on time at 9h30 (in seven oocytes with a fragmented chromosome, four matured on time; Fig. 7 B). This observation is fully consistent with previous work showing that drug-induced breakage of one bivalent does not induce SAC activation (Collins et al., 2015). Because we do not observe any delay in anaphase I timing in mCherry-Plk4 cRNA-injected oocytes (not depicted), which display higher Plk4 levels (Fig. 2, C and D), we conclude that it is not the presence of an excess active kinase but rather global perturbation of spindle assembly that delays meiosis I progression. As a consequence of

6h00; ****, P < 0.0001 (two-tailed *t* test with Welch correction); *n* is the number of oocytes. **(G)** Quantification of the percentage of oocytes with one broken bivalent in Plk4 OE line A and B observed at NEBD + 6h00; *, P = 0.0104 (Fisher's exact test); *N* is the number of mice, *n* is the number of oocytes. Error bars correspond to SD. **(H)** Scheme representing the positions of the two mCherry-Plk4 transgenes: the insertion (in blue) is closer to the centromeric region (in pink) of chromosome 9 for line A and the insertion (in green) is closer to the telomeric region of chromosome 12 for line B. **(I)** Two examples of FISH labeling of chromosome 9 (blue) in line A observed at NEBD + 6h00. 36 oocytes were collected from three mice. Among them, 16.67% had a broken bivalent. These broken bivalents were always labeled by the FISH probe for chromosome 9. DNA is labeled in gray. The FISH signal appears in blue. Scale bar is 10 µm for the left upper panel. Higher magnifications are shown in the middle and right upper panels; scale bar is 2 µm. Chromosome fragments labeled by the FISH probe appear in black on the right panels. **(J)** Proposed model of bivalent breakage occurring in the two Plk4 OE lines. MTs appear in dark green. Kinetochores are in pink. The mCherry-Plk4 transgene insertion sites appear in blue (line A) and green (line B).

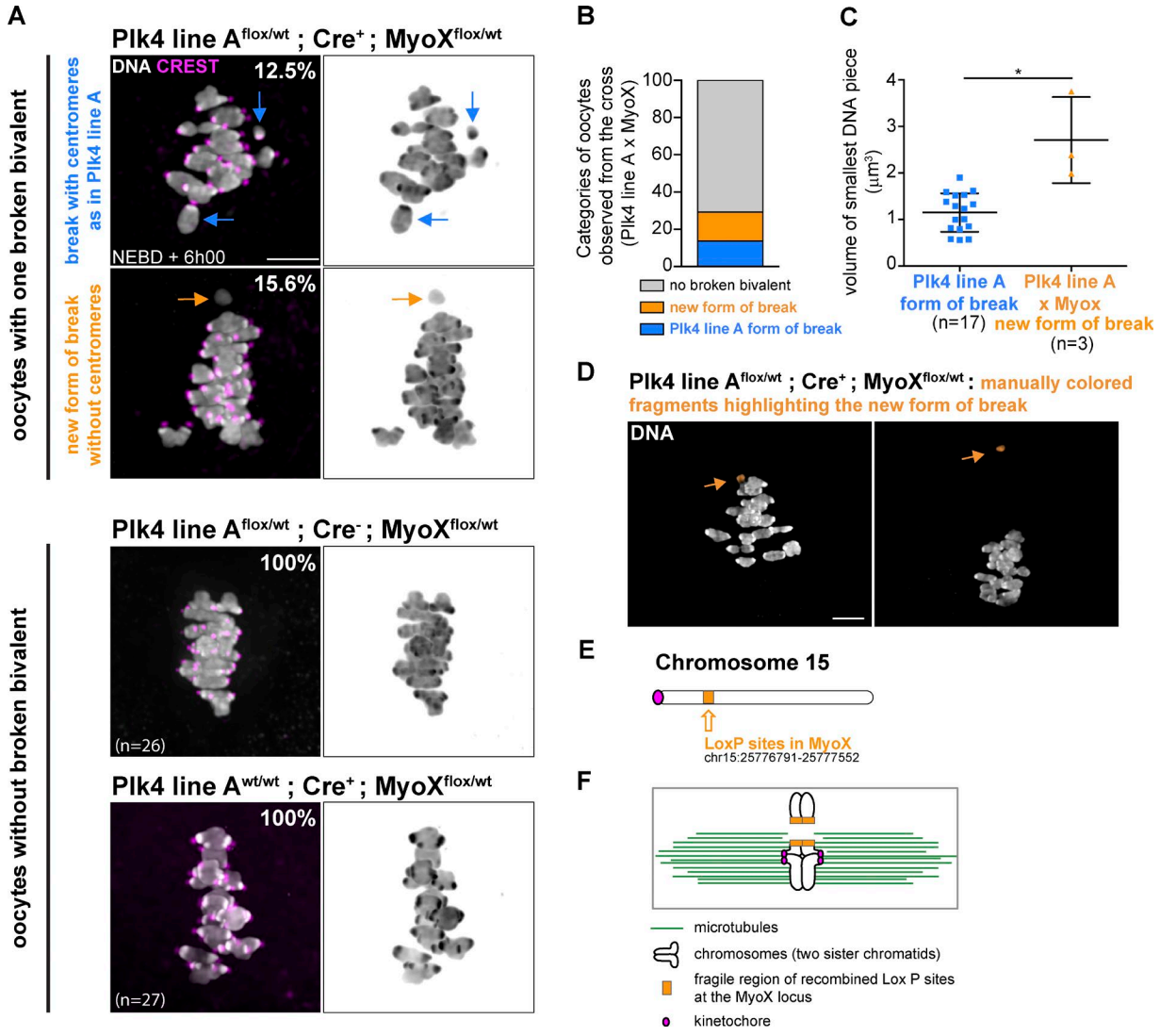

Figure 5. **The breakage is not specific to the Plk4 transgenic insertion. (A)** Oocytes coming from a Plk4 line A$^{flox/wt}$; Cre^{+}; MyoX$^{flox/wt}$ cross display both Plk4 line A type of break (12.5% of oocytes, upper panels, see blue arrows) and a new form of break producing a fragment with no centromeres (15.6% of oocytes, middle panels, see orange arrows). DNA is in gray levels and CREST is in magenta. The two lower panels show control oocytes (Plk4 line A$^{flox/wt}$; Cre^{-}; MyoX$^{flox/wt}$ and Plk4 line A$^{wt/wt}$; Cre^{+}; MyoX$^{flox/wt}$). The percentage of oocytes without broken bivalent from these controls is indicated on the pictures of the two left lower panels. Scale bar is 5 µm; *n* is the number of oocytes. **(B)** Percentages of oocytes with the different types of break in the Plk4 line A$^{flox/wt}$; Cre^{+}; MyoX$^{flox/wt}$ cross (on *n* = 32 oocytes). **(C)** Quantitative analysis of the volume of the smallest chromosome fragment in oocytes from Plk4 OE lines A (blue squares) and oocytes from the Plk4 line A$^{flox/wt}$; Cre^{+}; MyoX$^{flox/wt}$ cross (orange triangles) observed at NEBD + 6h00; *, P = 0.0121 (Mann–Whitney test); *n* is the number of oocytes. Error bars correspond to SD. **(D)** Examples of oocytes with the new type of broken bivalent in the Plk4 line A$^{flox/wt}$; Cre^{+}; MyoX$^{flox/wt}$ cross observed at NEBD + 6h00. Broken bivalents have been artificially colored in orange. Scale bar is 5 µm. **(E)** Scheme representing the position of the MyoX LoxP sites (orange) on chromosome 15. **(F)** Proposed model of the new bivalent breakage occurring in the Plk4 line A$^{flox/wt}$; Cre^{+}; MyoX$^{flox/wt}$ cross. MTs are in green. Kinetochores are in pink. The LoxP sites insertion region appears in orange.

this failure to arrest, some mature eggs will be produced with structural anomalies, as observed at anaphase I (Fig. 7 C).

Discussion

Fragmentation of aMTOCs at NEBD is normally concomitant with a burst in local MT assembly around chromosomes (Dumont et al., 2007; Schuh and Ellenberg, 2007). Here we found that precocious fragmentation of aMTOCs in conditions of Plk4 overexpression was associated with increased MT polymerization at NEBD. We showed that fragmentation of aMTOCs significantly increases their surface area, and so propose that augmentation of their capacity to polymerize MT is related to this surface area increase, providing larger sites for γ-TuRC recruitment. Previous work has shown that MT density controls the timing of first meiotic spindle bipolarization (Dumont et al., 2007; Breuer et al., 2010; Kolano et al., 2012). Consistent with this, Plk4 OE oocytes displayed accelerated rates of spindle bipolarization. In mouse oocytes, the aMTOC morphology appears adapted to mediate the nucleation of an appropriate amount of MT at a given time, and we show here that alterations from this timely regulation have deleterious consequences on meiosis outcome.

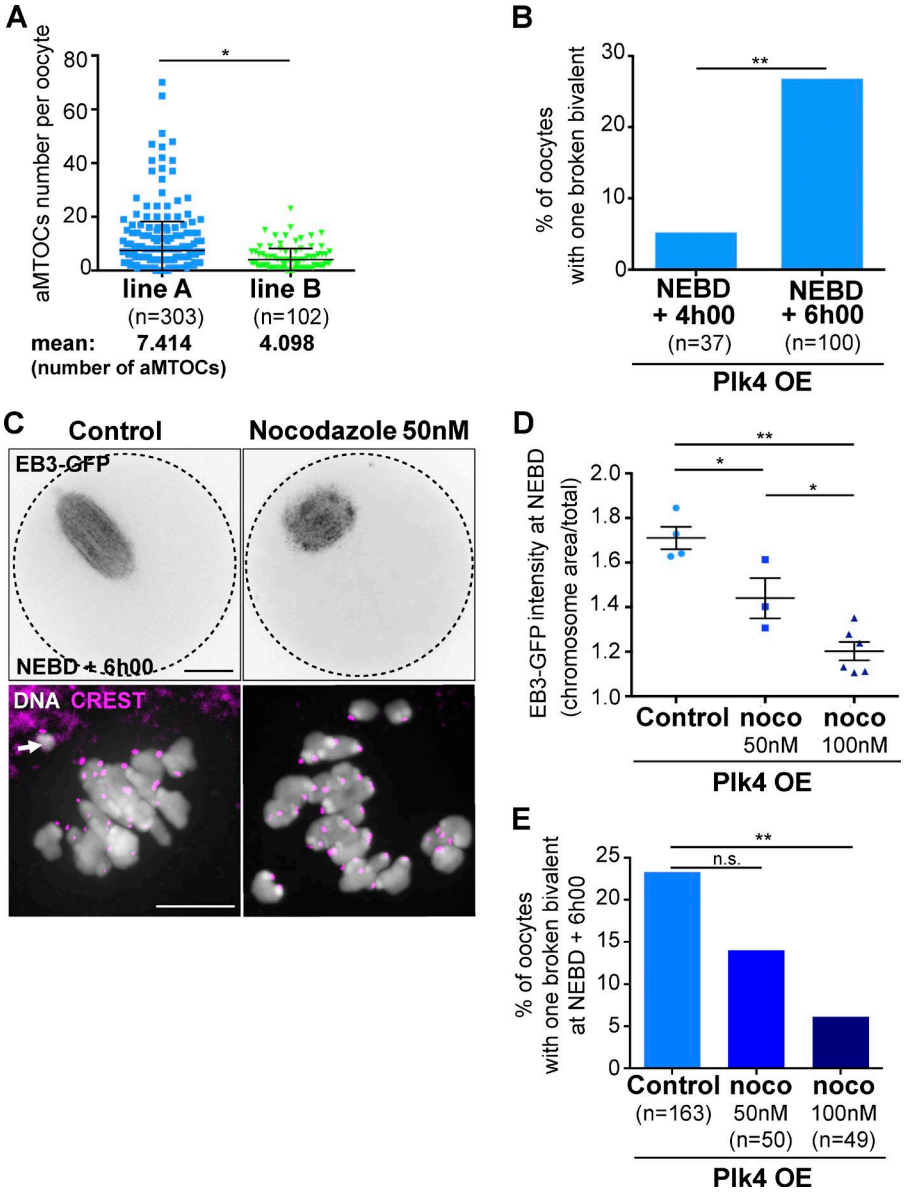

Figure 6. **Extent of bivalent breakage correlates with aMTOC spreading and MT density. (A)** Quantitative analysis of aMTOC number per oocyte in the two Plk4 OE lines (line A, blue squares, and line B, green triangles) in prophase I; *, P = 0.0365 (two-tailed Mann–Whitney test). The mean number of aMTOCs per prophase I oocyte is indicated below the graph for each line. **(B)** Extent of bivalent breakage increases significantly as meiosis I progresses in oocytes from line A. Percentage of Plk4 OE oocytes from line A with one broken bivalent as a function of the stage of meiosis I (NEBD + 4h00 and NEBD + 6h00); **, P = 0.0047. **(C)** Effect of 50 nM nocodazole treatment observed at NEBD + 6h00 in living Plk4 OE oocytes from line A, expressing EB3-GFP (upper panels) and in fixed samples (lower panels) labeled for DNA (white) and CREST (pink). The black dotted circles in the upper panels highlight the oocyte contour. Scale bar is 20 µm. **(D)** Quantification of the relative MT density measured at NEBD around chromosomes in Plk4 OE from line A oocytes injected with EB3-GFP in control conditions or after treatment with 50 or 100 nM nocodazole (noco). The EB3-GFP signal was measured in a Ø20-µm region around the chromosomes; total signal intensity was measured in a Ø70-µm region covering the whole oocyte. Normalized signal intensity is the ratio of local/total intensity measured for individual oocytes. Tukey's multiple comparison test gives *, P < 0.05 for controls vs. noco 50 nM; **, P < 0.01 for controls vs. noco 100 nM; and *, P < 0.05 for noco 50 nM vs. noco 100 nM. **(E)** Decreasing MT density with nocodazole reduces the extent of DNA breakage. Percentage of Plk4 OE oocytes from line A presenting one broken bivalent at NEBD + 6h00 as a function of nocodazole concentration (0, 50, and 100 nM, respectively, darker blue histograms). P = 0.1725 for 0 vs. 50 nM, and **, P = 0.0068 for 0 vs. 100 nM. For B and E, the statistical tests used are Fisher's exact tests. For A, B, and E, *n* is the number of oocytes. Error bars correspond to SD.

We observe that spindles assembled with higher MT density at NEBD correlated with the presence of three different broken chromosomes (chromosome 9 and probably also 12 and 15) in different regions, near centromeres or close to telomeres (Fig. S3 C). The capacity of spindle MT to exert sufficient tension on chromosomes resulting in their breakage is still a matter of debate (Ganem and Pellman, 2012). However, here we provide evidence that this can happen in meiosis in regions where a Cre-mediated recombination event may have generated a region of fragility. The mechanism at the origin of this fragility remains elusive, and we cannot exclude that Plk4 overexpression during oocyte growth may have favored a fragility that is revealed only after meiosis resumption. However, it is rather unlikely that the break occurred before meiosis resumption, since Plk4 OE oocytes at all stages of their growth from both transgenic lines displayed overexpression of the mCherry-Plk4 transgene (data not shown). These data argue that Cre-mediated recombination and repair occurred in all oocytes, at the beginning of their growth phase, when the ZP3-Cre turns on (Lewandoski et al., 1997) to allow Plk4 transgene expression. Furthermore, the percentage of oocytes presenting one broken bivalent increased significantly (5×) from 4h00 to 6h00 after NEBD (Fig. 6 B). Our data thus suggest that most breaks are revealed while the meiosis I spindle is being assembled (Fig. S5). Meiosis I spindle assembly in both mouse and human oocytes is progressive, starting with the setup of bipolarity, then K-fiber assembly around NEBD + 5h00, and ending with spindle poles assembly (Dumont et al., 2007; Schuh and Ellenberg, 2007; Breuer et al., 2010; Kitajima et al., 2011; Holubcová et al., 2015; Bennabi et al., 2016). Even though forces during the different critical steps of meiosis I spindle assembly have never been measured directly, we can speculate that these forces increase as more bundles are made and K-fibers become progressively solidly anchored into the two spindle poles. This could potentially explain the increase in breakage events observed in our model.

In mitosis, the consequences of Plk4 overexpression have been extensively studied in various model systems (Habedanck et al.,

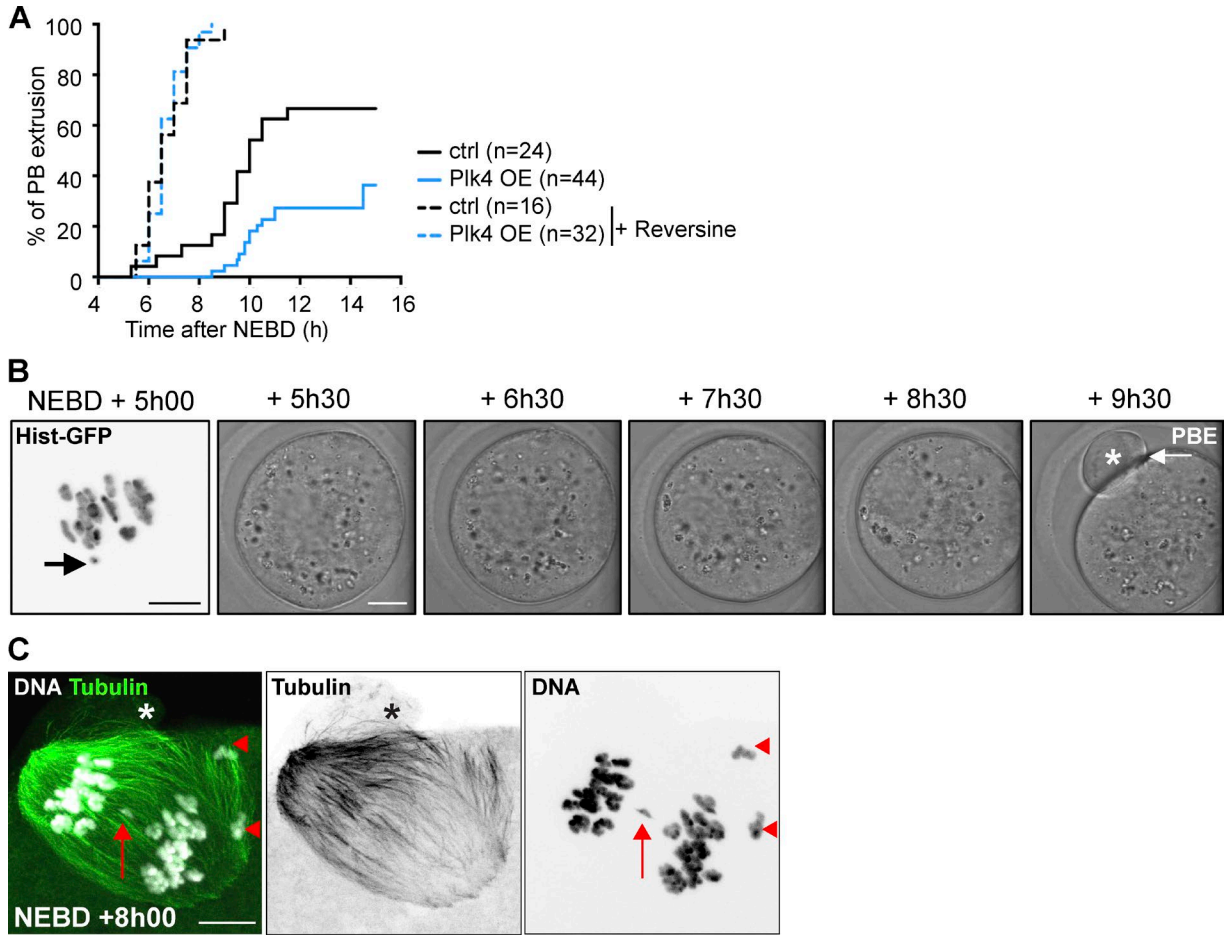

Figure 7. **Plk4 OE oocytes have impaired progression into meiosis I owing to SAC activation. (A)** Kinetics of PBE extrusion in controls (black curves) and Plk4 OE (blue curves) oocytes from line A upon treatment (dotted curves) or not (plain curves) with 100 nM Reversine at NEBD; *n* is the number of oocytes; PBE mean times are 9h05 for controls, 10h50 for Plk4 OE, 6h43 for controls treated by Reversine, and 6h41 for Plk4 OE treated by Reversine. Tukey's multiple comparison test: **, P < 0.01 for controls vs. Plk4 OE; ****, P < 0.0001 for controls vs. controls + Reversine, controls vs. Plk4 OE + Reversine, Plk4 OE vs. controls + Reversine, and Plk4 OE vs. Plk4 OE + Reversine. Controls + Reversine and Plk4 OE + Reversine are not significantly different. **(B)** Live image of a Plk4 OE oocyte (line A) presenting a DNA fragment (chromosomes labeled with histone-GFP) which can be observed on the left picture (black arrow) and that nonetheless extrudes a first polar body at NEBD + 9h30 (PBE, white arrow and white star). Scale bar is 10 µm for the left panel and 20 µm for the other panels. Time points are in hours and minutes after NEBD. The emerging first polar body is highlighted by a white star. **(C)** Evidence for structural defects in chromosome segregation in Plk4 OE oocytes. Plk4 OE oocyte from line A, observed at NEBD + 8h00, undergoing anaphase I where DNA (white) and MT (green) are labeled. We can clearly observe the smallest DNA fragment lagging in between the two sets of univalents (red arrow) and the largest DNA fragment being separated into two deleted univalents, each retained in the oocyte (two red arrowheads). The stars indicate the position of the polar body starting to be emitted. Scale bar is 10 µm.

2005; Rodrigues-Martins et al., 2007; Marthiens et al., 2013), but with no reported evidence for Plk4-induced chromosome breaks. Furthermore, whole-genome sequencing of Plk4 OE cells from several mouse tissues have not identified acentric chromosomes (Serçin et al., 2016; Levine et al., 2017). One main difference between previous studies and ours is that in mitotic spindles, forces are mostly exerted on kinetochores, whereas in meiosis, spindle forces exerted on kinetochores are transmitted to chiasmata and to chromosome arms. This suggests that the specific architecture of meiosis I chromosomes, bivalents held by chiasmata, might be more susceptible to break under potentially increased spindle forces, in condition of fragility (Figs. 4 J and 5 F). Yet, another important difference between meiosis and mitosis, is the extensive duration of meiosis I in mouse (8 to 9 h) and human (up to 17 h) oocytes (Holubcová et al., 2015; Bennabi et al., 2016) compared with mitosis (2 h). Indeed, it is known that weak forces applied repetitively can efficiently break DNA in vitro (Liang et al., 2013). The extended length of meiosis I of mammalian oocytes might favor the occurrence of such breaks.

Importantly, the presence of these breaks, in particular those producing acentric chromatin fragments not retained in the spindle (in Plk4 OE from line B and in Plk4 line A × MyoX), will not be detected by the SAC, as it functions through detecting MT occupancy at the kinetochore. Hence kinetochore-free chromatin is not recognized by any component of this checkpoint pathway. The other type of break we describe in line A will not be sufficient to elicit a robust SAC response (our results and Collins et al., 2015). Both types will lead to a class of chromosome abnormalities in the resulting egg that have not been observed during meiosis I before without prior treatment with DNA-damaging agents. Yet such types of structural anomalies, where terminal small pieces of chromosomes are missing, are quite frequent,

from 1/20,000 to 1/50,000 for Wolf–Hirschhorn syndrome (Ho et al., 2016). It would be interesting to investigate the status of Plk4 activity in Wolf–Hirschhorn syndrome, as affected children are precisely characterized by mutations in the Plk4 gene (Martin et al., 2014). Even though we describe here a very artificial system, our work might shed new light on the etiology of human diseases associated with terminal deletions.

Materials and methods

Mouse strains and genotyping

Zp3-Cre [C57BL/6-Tg(Zp3-cre)93Knw/J] breeding pairs were obtained from the Jackson Laboratory. mCherry-Plk4$^{flox/wt}$ mice were generated by random insertion of a pCAG-loxCAT-lox-mCherryPlk4SV40pA construct in the genome of C57BL/6N mice (Marthiens et al., 2013). Two transgenic lines were amplified from two different founder lines with two different insertion sites and different transgene copy number and are referred to, for simplicity, as line A and B. Line A corresponds to the F3 line in Marthiens et al. (2013). Unless specified, most experiments were performed on line A, which presented a higher extent of aMTOC fragmentation and DNA breakage. For detection of Cre-mediated multiple stop codon excision, genotyping was performed using the following primers: for the Cre, 5′-GCGGTCTGGCAGTAAAAA CTATC-3′ and 5′-GTGAAACAGCATTGCTGTCACTT-3′; and for the mCherry, 5′-CGCCACCATGGTGAGCAAGGG-3′ and 5′-CTC GTCCATGCCGCCGGTGG-3′. Control oocytes came from either Plk4$^{flox/wt}$; Cre^{-} or Plk4$^{wt/wt}$; Cre^{+} female mice, while Plk4 OE oocytes came from Plk4$^{flox/wt}$; Cre^{+} female mice. In Fig. 5, we also used oocytes coming from a cross of the Plk4 line A$^{flox/wt}$; Cre^{+} with the MyoX$^{flox/wt}$; Cre^{-} mice. The MyoX$^{flox/wt}$; Cre^{-} have been constructed by Genoway by insertion of two Lox P sites between exons 26 and 30 of the Myosin X endogenous locus (Fig. S3 B).

Transgene integration sites identification

Target locus amplification and next-generation sequencing, made by Cergentis, were used to determine the transgenic single-stranded oligodeoxynucleotide integration sites as previously described (de Vree et al., 2014).

Oocyte collection and culture

Oocytes were collected from 8- to 12-wk-old female mice into M2 + BSA medium supplemented with 1 µM milrinone (Reis et al., 2006) to ensure a block in prophase I. Resumption of meiosis was triggered by culturing oocytes in milrinone-free medium. All drugs were stored in DMSO at −20°C and diluted in M2 + BSA.

Plasmid construction and in vitro transcription of cRNA

We used previously described constructs, pRN3-H2B-RFP, pRN3-EB3-GFP (Breuer et al., 2010), and pMDL-Mad2-YFP (Lane et al., 2012). Histone2B-GFP (a gift from G. Halet, Institut de Génétique et Développement de Rennes, Rennes, France) was subcloned into the pRN3 vector. The mCherry-Plk4 construct used to produce the transgenic lines (Marthiens et al., 2013) was subcloned into the pRN3 vector. All cRNAs were synthesized using the T3 mMessage mMachine kit (Ambion) and resuspended in RNase-free water as previously described (Verlhac et al., 2000).

Microinjection

Injection of in vitro–transcribed cRNAs into the cytoplasm of prophase I–arrested oocytes was performed using an Eppendorf Femtojet microinjector as described (Verlhac et al., 2000) and the oocytes were further kept for 1–3 h in milrinone to allow expression of fusion proteins. Oocytes were then released from their prophase I arrest by transferring and washing into milrinone-free M2 medium.

Drug treatments

Both nocodazole and reversine were added at NEBD. Oocytes were collected in M2 medium + milrinone and then washed in milrinone-free M2 medium containing either 50 or 100 nM nocodazole or 100 nM reversine as in Hached et al. (2011) and Kolano et al. (2012). Oocytes were kept in nocodazole until fixation at NEBD + 6h00. Control oocytes were treated with DMSO at the same dilution as the drugs.

Live imaging

Spinning disk videos were acquired using a Plan APO 40×/1.25-NA objective on a Leica DMI6000B microscope, enclosed in a thermostatic chamber set at 37°C (Life Imaging Services) and equipped with a CoolSnap HQ2/CCD-camera (Princeton Instruments) or EMCCD camera (Evolve) coupled to a Sutter filter wheel (Roper Scientific) and a Yokogawa CSU-X1-M1 confocal scanner. MetaMorph software (Universal Imaging) was used to collect the data.

Immunofluorescence

For MT observations, oocytes were fixed using glutaraldehyde as previously described (Terret et al., 2003). For Plk4 endogenous labeling, oocytes were fixed using ice-cold (−20°C) methanol for 10 min. For CREST staining, oocytes were fixed at 30°C for 30 min in PHEM (Pipes, Hepes, EGTA, and $MgCl_2$) buffer containing 2% formaldehyde and 0.05% Triton X-100, and were then permeabilized for 10 min in PBS containing 0.05% Triton X-100. Oocytes were extensively washed with PBS buffer between solutions. Oocytes were incubated at 4°C overnight in PBS supplemented with Tween-20 before primary antibody incubation (CREST, Abcam, 1:50). We used a rat monoclonal antibody against tyrosinated α-tubulin (YL1/2, Abcam) at 1:200 and mouse monoclonal anti-pericentrin (BD) at 1:400. For Plk4 labeling, a rabbit anti-Plk4 antibody was used at 1:500 (gift of A. Holland, John Hopkins School of Medicine, Baltimore, MD). After primary antibody incubation and subsequent washes, oocytes were labeled with the corresponding secondary antibodies (Jackson ImmunoResearch Laboratories). Coverslips were mounted in Prolong Gold with DAPI (Life Technologies). SIM samples were treated with lower concentrations of antibodies to avoid signal saturation and mounted in Prolong Gold without DAPI.

Image acquisition of fixed oocytes was performed on the SP5/AOBS confocal microscope equipped with a Plan APO 63×/1.4-NA objective or on the Spinning disc used for live imaging, and deconvolution was applied using Huygens software (SVI).

SIM acquisitions were performed on workstations of the Nikon Imaging Centre of the Curie Institute. Acquisitions were performed in 3D SIM mode with an n-SIM Nikon microscope

before image reconstruction using NIS-Elements software based on Schermelleh et al. (2008). The system is equipped with an APO TIRF100 1.49-NA oil immersion and an EMCCD DU-897 Andor camera.

DNA-FISH

Oocytes were cultured in M2 medium and fixed once in 1× PBS, 1% PFA, and 1 mg/ml polyvinylpyrrolidone (PVP), for 1 min at RT. Cells were permeabilized at RT for 1 min in 1× PBS, 0.4% Triton X-100, and 0.5% PFA. Cells were further fixed for 10 min at RT in 1× PBS, 4% PFA, 1 mg/ml PVP, and 0.05% Triton X-100. Cells were then permeabilized in 1× PBS, 0.5% Triton X-100, 1 mg/ml PVP, and 0.02% RNase for 1 h at 37°C. Samples were preincubated in 1 µg/ml Cot-1 DNA, 10% dextran sulfate, 2× SSC, 0.5 mM EDTA, 0.05% Triton X-100, 1 mg/ml PVP, 0.5 mg/ml BSA, and 4 M urea, pH 7.3, overnight at 37°C, then denatured at 83°C for 10 min and prehybridized for 1 h at 37°C. Here urea has been used instead of formamide (Sinigaglia et al., 2018). After overnight hybridization with a chromosome paint against chromosome 9 (Metasystem, see supplier's protocol) at 37°C, oocytes were washed at 45° twice for 15 min in 0.2× SSC, 0.05% Triton X-100, and 1 mg/ml PVP and mounted in Prolong Gold with DAPI (Life Technologies). Denaturation and hybridization steps were performed in glass-bottom Petri dishes. Other steps were performed in 4% agarose and 9 mg/ml NaCl-coated Petri dishes.

Image analysis

3D analysis of aMTOCs and chromosome fragment morphology was performed using Imaris (Bitplane). Thresholding of objects was done in a semiautomatic way. First, objects were thresholded automatically via Imaris, then we checked the accuracy of the threshold manually. Comparison of mCherry-Plk4 overexpression levels in cRNA-injected oocytes versus transgenic oocytes was performed in Metamorph by measuring the absolute intensity of fluorescence on summed Z-projections (70 Z, spaced every 0.5 µm, arbitrary units). Background values were measured within a region of interest outside the cell and were subtracted before quantification. Plk4 and pericentrin levels in Plk4OE oocytes over endogenous protein in control oocytes were quantified on summed Z-projections (70 Z, spaced every 0.5 µm, arbitrary units). SIM acquisitions were treated in Fiji after reconstruction and realignment then rendered in Imaris 3D viewer after calibration. The total and local MT fluorescence signal intensities were measured in oocytes expressing EB3-GFP on summed Z-stack projections (six Z planes spaced every 4 µm). Timing of bipolarization was assessed in oocytes expressing EB3-GFP imaged at 10-min intervals.

Statistical analyses were performed using Graphpad Prism 5.0 software. ns, nonsignificant ($P > 0.05$); *, $P < 0.05$; **, $P < 0.01$; ***, $P < 0.001$; and ****, $P < 0.0001$.

Online supplemental material

Fig. S1 shows quantification of the pericentrin and Plk4 signals in the whole oocyte and SIM acquisition of aMTOCs in Plk4 OE oocytes. Fig. S2 shows that Plk4OE oocytes present accelerated rates of spindle bipolarization as observed in fixed oocytes. Fig. S3 illustrates the different genetic insertions used in the study. Fig. S4 shows that the amount of mCherry-Plk4 on aMTOCs is comparable in line A and B in prophase I oocytes. Fig. S5 shows a scheme recapitulating our model. Video 1 shows that spindle bipolarization is accelerated in oocytes overexpressing Plk4. Video 2 shows a chromosome fragment moving back and forth across the metaphase plate in Plk4OE oocyte. Video 3 shows 20 bivalents observed in control oocytes at NEBD +6h00. Video 4 shows 21 pieces of DNA counted in Plk4 OE line A oocytes at NEBD +6h00. Video 5 shows 21 pieces of DNA counted in Plk4 OE line B oocytes at NEBD +6h00. Video 6 shows that a new form of DNA break can be observed in Plk4 line $A^{flox/wt}$; Cre^{+}; $MyoX^{flox/wt}$ oocytes at NEBD +6h00. Video 7 shows that bivalents can be easily counted in Plk4 OE oocytes observed at NEBD +4h00. Video 8 shows that bivalents can be easily counted in Plk4 OE oocytes treated with 50 nM nocodazole and observed at NEBD +6h00.

Acknowledgments

We thank Ludovic Dumont and Anchi Chang, masters students, for their help at the beginning of the project; Carole Pennetier and Manon Chartier at the Curie Institute for genotyping; Adel Al Jord from our laboratory for critical reading of the manuscript; Lucie Sengmanivong from the Nikon Imaging Centre at Institut Curie-Centre National de la Recherche Scientifique (Paris, France); Guillaume Halet for the gift of the HistoneH2B-GFP plasmid; Andrew Holland for the gift of the anti-Plk4 antibody; and Katia Ancelin and Edith Heard at the Curie Institute for the DNA-FISH protocol.

M. Łuksza was supported by a Fondation ARC pour la Recherche sur le Cancer fellowship. This work was supported by a grant from the Ligue Contre le Cancer (EL/2012/LNCC/MHV), the Agence Nationale de la Recherche (ANR-DIVACEN to M.-H. Verlhac and R. Basto, 14-CE11), a Fondation pour la Recherche Médicale Label (DEQ20150331758 to M.-H. Verlhac), and an Institut National du Cancer grant (PLBIO 2016-270-TRAN). This work has received support from the Fondation Bettencourt Schueller, support under the program "Investissements d'Avenir" launched by the French government and implemented by the Agence Nationale de la Recherche (ANR-10-LABX-54 MEMO LIFE, ANR-11-IDEX-0001-02 PSL* Research University). The work was also supported by Biotechnology and Biological Sciences Research Council funding to K.T. Jones (Mechanisms of DNA damage and repair in mature oocytes, BBSRC, BB/L006006/1) and American Institute for Cancer Research (now Worldwide Cancer Research; 13-0170) to V. Marthiens and R. Basto.

The authors declare no competing financial interests.

Author contributions: M. Manil-Ségalen and M.-H. Verlhac conceived and supervised the project. M. Manil-Ségalen performed most experiments. M. Łuksza and J. Kanaan participated in some experiments. M. Manil-Ségalen and M.-H. Verlhac analyzed most experiments. S.I.R. Lane and K.T. Jones performed the mad2-YFP experiment. V. Marthiens, M.-E. Terret, and R. Basto provided scientific input, mouse strains, and reagents. M. Manil-Ségalen and M.-H. Verlhac wrote the manuscript, which was seen and corrected by all authors.

Submitted: 12 June 2018
Revised: 16 July 2018
Accepted: 20 July 2018

References

Bennabi, I., M.-E. Terret, and M.-H. Verlhac. 2016. Meiotic spindle assembly and chromosome segregation in oocytes. *J. Cell Biol.* 215:611–619. https://doi.org/10.1083/jcb.201607062

Bettencourt-Dias, M., A. Rodrigues-Martins, L. Carpenter, M. Riparbelli, L. Lehmann, M.K. Gatt, N. Carmo, F. Balloux, G. Callaini, and D.M. Glover. 2005. SAK/PLK4 is required for centriole duplication and flagella development. *Curr. Biol.* 15:2199–2207. https://doi.org/10.1016/j.cub.2005.11.042

Breuer, M., A. Kolano, M. Kwon, C.-C. Li, T.-F. Tsai, D. Pellman, S. Brunet, and M.-H. Verlhac. 2010. HURP permits MTOC sorting for robust meiotic spindle bipolarity, similar to extra centrosome clustering in cancer cells. *J. Cell Biol.* 191:1251–1260. https://doi.org/10.1083/jcb.201005065

Brunet, S., G. Pahlavan, S. Taylor, and B. Maro. 2003. Functionality of the spindle checkpoint during the first meiotic division of mammalian oocytes. *Reproduction.* 126:443–450. https://doi.org/10.1530/rep.0.1260443

Bury, L., P.A. Coelho, A. Simeone, S. Ferries, C.E. Eyers, P.A. Eyers, M. Zernicka-Goetz, and D.M. Glover. 2017. Plk4 and Aurora A cooperate in the initiation of acentriolar spindle assembly in mammalian oocytes. *J. Cell Biol.* 216:3571–3590. https://doi.org/10.1083/jcb.201606077

Cimini, D., B. Howell, P. Maddox, A. Khodjakov, F. Degrassi, and E.D. Salmon. 2001. Merotelic kinetochore orientation is a major mechanism of aneuploidy in mitotic mammalian tissue cells. *J. Cell Biol.* 153:517–527. https://doi.org/10.1083/jcb.153.3.517

Clift, D., and M. Schuh. 2015. A three-step MTOC fragmentation mechanism facilitates bipolar spindle assembly in mouse oocytes. *Nat. Commun.* 6:7217. https://doi.org/10.1038/ncomms8217

Coelho, P.A., L. Bury, B. Sharif, M.G. Riparbelli, J. Fu, G. Callaini, D.M. Glover, and M. Zernicka-Goetz. 2013. Spindle formation in the mouse embryo requires Plk4 in the absence of centrioles. *Dev. Cell.* 27:586–597. https://doi.org/10.1016/j.devcel.2013.09.029

Collins, J.K., S.I.R. Lane, J.A. Merriman, and K.T. Jones. 2015. DNA damage induces a meiotic arrest in mouse oocytes mediated by the spindle assembly checkpoint. *Nat. Commun.* 6:8553–8565. https://doi.org/10.1038/ncomms9553

Crasta, K., N.J. Ganem, R. Dagher, A.B. Lantermann, E.V. Ivanova, Y. Pan, L. Nezi, A. Protopopov, D. Chowdhury, and D. Pellman. 2012. DNA breaks and chromosome pulverization from errors in mitosis. *Nature.* 482:53–58. https://doi.org/10.1038/nature10802

de Vree, P.J.P., E. de Wit, M. Yilmaz, M. van de Heijning, P. Klous, M.J.A.M. Verstegen, Y. Wan, H. Teunissen, P.H.L. Krijger, G. Geeven, et al. 2014. Targeted sequencing by proximity ligation for comprehensive variant detection and local haplotyping. *Nat. Biotechnol.* 32:1019–1025. https://doi.org/10.1038/nbt.2959

Dumont, J., and A. Desai. 2012. Acentrosomal spindle assembly and chromosome segregation during oocyte meiosis. *Trends Cell Biol.* 22:241–249. https://doi.org/10.1016/j.tcb.2012.02.007

Dumont, J., S. Petri, F. Pellegrin, M.-E. Terret, M.T. Bohnsack, P. Rassinier, V. Georget, P. Kalab, O.J. Gruss, and M.-H. Verlhac. 2007. A centriole- and RanGTP-independent spindle assembly pathway in meiosis I of vertebrate oocytes. *J. Cell Biol.* 176:295–305. https://doi.org/10.1083/jcb.200605199

Etemad, B., and G.J.P.L. Kops. 2016. Attachment issues: kinetochore transformations and spindle checkpoint silencing. *Curr. Opin. Cell Biol.* 39:101–108. https://doi.org/10.1016/j.ceb.2016.02.016

Fu, J., and D.M. Glover. 2012. Structured illumination of the interface between centriole and peri-centriolar material. *Open Biol.* 2:120104. https://doi.org/10.1098/rsob.120104

Ganem, N.J., and D. Pellman. 2012. Linking abnormal mitosis to the acquisition of DNA damage. *J. Cell Biol.* 199:871–881. https://doi.org/10.1083/jcb.201210040

Ganem, N.J., S.A. Godinho, and D. Pellman. 2009. A mechanism linking extra centrosomes to chromosomal instability. *Nature.* 460:278–282. https://doi.org/10.1038/nature08136

Habedanck, R., Y.-D. Stierhof, C.J. Wilkinson, and E.A. Nigg. 2005. The Polo kinase Plk4 functions in centriole duplication. *Nat. Cell Biol.* 7:1140–1146. https://doi.org/10.1038/ncb1320

Hached, K., S.Z. Xie, E. Buffin, D. Cladière, C. Rachez, M. Sacras, P.K. Sorger, and K. Wassmann. 2011. Mps1 at kinetochores is essential for female mouse meiosis I. *Development.* 138:2261–2271. https://doi.org/10.1242/dev.061317

Heald, R., R. Tournebize, T. Blank, R. Sandaltzopoulos, P. Becker, A. Hyman, and E. Karsenti. 1996. Self-organization of microtubules into bipolar spindles around artificial chromosomes in Xenopus egg extracts. *Nature.* 382:420–425. https://doi.org/10.1038/382420a0

Ho, K.S., S.T. South, A. Lortz, C.H. Hensel, M.R. Sdano, R.J. Vanzo, M.M. Martin, A. Peiffer, C.G. Lambert, A. Calhoun, et al. 2016. Chromosomal microarray testing identifies a 4p terminal region associated with seizures in Wolf-Hirschhorn syndrome. *J. Med. Genet.* 53:256–263. https://doi.org/10.1136/jmedgenet-2015-103626

Holubcová, Z., M. Blayney, K. Elder, and M. Schuh. 2015. Human oocytes. Error-prone chromosome-mediated spindle assembly favors chromosome segregation defects in human oocytes. *Science.* 348:1143–1147. https://doi.org/10.1126/science.aaa9529

Kitajima, T.S., M. Ohsugi, and J. Ellenberg. 2011. Complete kinetochore tracking reveals error-prone homologous chromosome biorientation in mammalian oocytes. *Cell.* 146:568–581. https://doi.org/10.1016/j.cell.2011.07.031

Kolano, A., S. Brunet, A.D. Silk, D.W. Cleveland, and M.-H. Verlhac. 2012. Error-prone mammalian female meiosis from silencing the spindle assembly checkpoint without normal interkinetochore tension. *Proc. Natl. Acad. Sci. USA.* 109:E1858–E1867. https://doi.org/10.1073/pnas.1204686109

Lane, S.I.R., Y. Yun, and K.T. Jones. 2012. Timing of anaphase-promoting complex activation in mouse oocytes is predicted by microtubule-kinetochore attachment but not by bivalent alignment or tension. *Development.* 139:1947–1955. https://doi.org/10.1242/dev.077040

Lane, S.I.R., S.L. Morgan, T. Wu, J.K. Collins, J.A. Merriman, E. ElInati, J.M. Turner, and K.T. Jones. 2017. DNA damage induces a kinetochore-based ATM/ATR-independent SAC arrest unique to the first meiotic division in mouse oocytes. *Development.* 144:3475–3486. https://doi.org/10.1242/dev.153965

Lawo, S., M. Hasegan, G.D. Gupta, and L. Pelletier. 2012. Subdiffraction imaging of centrosomes reveals higher-order organizational features of pericentriolar material. *Nat. Cell Biol.* 14:1148–1158. https://doi.org/10.1038/ncb2591

Levine, M.S., B. Bakker, B. Boeckx, J. Moyett, J. Lu, B. Vitre, D.C. Spierings, P.M. Lansdorp, D.W. Cleveland, D. Lambrechts, et al. 2017. Centrosome amplification is sufficient to promote spontaneous tumorigenesis in mammals. *Dev. Cell.* 40:313–322.e5. https://doi.org/10.1016/j.devcel.2016.12.022

Lewandoski, M., K.M. Wassarman, and G.R. Martin. 1997. Zp3-cre, a transgenic mouse line for the activation or inactivation of loxP-flanked target genes specifically in the female germ line. *Curr. Biol.* 7:148–151. https://doi.org/10.1016/S0960-9822(06)00059-5

Liang, H., N. Severin, S. Fugmann, I.M. Sokolov, and J.P. Rabe. 2013. Statistics of time-dependent rupture of single ds-DNA. *J. Phys. Chem. B.* 117:8875–8879. https://doi.org/10.1021/jp400872k

Luksza, M., I. Queguigner, M.-H. Verlhac, and S. Brunet. 2013. Rebuilding MTOCs upon centriole loss during mouse oogenesis. *Dev. Biol.* 382:48–56. https://doi.org/10.1016/j.ydbio.2013.07.029

Marangos, P., M. Stevense, K. Niaka, M. Lagoudaki, I. Nabti, R. Jessberger, and J. Carroll. 2015. DNA damage-induced metaphase I arrest is mediated by the spindle assembly checkpoint and maternal age. *Nat. Commun.* 6:8706. https://doi.org/10.1038/ncomms9706

Maro, B., S.K. Howlett, and M. Webb. 1985. Non-spindle microtubule organizing centers in metaphase II-arrested mouse oocytes. *J. Cell Biol.* 101:1665–1672. https://doi.org/10.1083/jcb.101.5.1665

Marthiens, V., M.A. Rujano, C. Pennetier, S. Tessier, P. Paul-Gilloteaux, and R. Basto. 2013. Centrosome amplification causes microcephaly. *Nat. Cell Biol.* 15:731–740. https://doi.org/10.1038/ncb2746

Martin, C.-A., I. Ahmad, A. Klingseisen, M.S. Hussain, L.S. Bicknell, A. Leitch, G. Nürnberg, M.R. Toliat, J.E. Murray, D. Hunt, et al. 2014. Mutations in PLK4, encoding a master regulator of centriole biogenesis, cause microcephaly, growth failure and retinopathy. *Nat. Genet.* 46:1283–1292. https://doi.org/10.1038/ng.3122

Mennella, V., B. Keszthelyi, K.L. McDonald, B. Chhun, F. Kan, G.C. Rogers, B. Huang, and D.A. Agard. 2012. Subdiffraction-resolution fluorescence microscopy reveals a domain of the centrosome critical for pericentriolar material organization. *Nat. Cell Biol.* 14:1159–1168. https://doi.org/10.1038/ncb2597

Morgan, A.P., D.M. Gatti, M.L. Najarian, T.M. Keane, R.J. Galante, A.I. Pack, R. Mott, G.A. Churchill, and F.P.-M. de Villena. 2017. Structural variation shapes the landscape of recombination in mouse. *Genetics.* 206:603–619. https://doi.org/10.1534/genetics.116.197988

Nagaoka, S.I., C.A. Hodges, D.F. Albertini, and P.A. Hunt. 2011. Oocyte-specific differences in cell-cycle control create an innate susceptibility to meiotic errors. *Curr. Biol.* 21:651–657. https://doi.org/10.1016/j.cub.2011.03.003

Okten, G., O. Sezer, S. Günes, S. Küçüködük, and G. Oğur. 2009. Two cases of 9p deletion syndrome and a case of partial trisomy 8 and partial monosomy 9p. *Genet. Couns.* 20:341–347.

Reis, A., H.-Y. Chang, M. Levasseur, and K.T. Jones. 2006. APCcdh1 activity in mouse oocytes prevents entry into the first meiotic division. *Nat. Cell Biol.* 8:539–540. https://doi.org/10.1038/ncb1406

Rieder, C.L., and H. Maiato. 2004. Stuck in division or passing through: what happens when cells cannot satisfy the spindle assembly checkpoint. *Dev. Cell.* 7:637–651. https://doi.org/10.1016/j.devcel.2004.09.002

Rieder, C.L., and R.E. Palazzo. 1992. Colcemid and the mitotic cycle. *J. Cell Sci.* 102:387–392.

Rodrigues-Martins, A., M. Riparbelli, G. Callaini, D.M. Glover, and M. Bettencourt-Dias. 2007. Revisiting the role of the mother centriole in centriole biogenesis. *Science.* 316:1046–1050. https://doi.org/10.1126/science.1142950

Sacristan, C., and G.J.P.L. Kops. 2015. Joined at the hip: kinetochores, microtubules, and spindle assembly checkpoint signaling. *Trends Cell Biol.* 25:21–28. https://doi.org/10.1016/j.tcb.2014.08.006

Schermelleh, L., P.M. Carlton, S. Haase, L. Shao, L. Winoto, P. Kner, B. Burke, M.C. Cardoso, D.A. Agard, M.G.L. Gustafsson, et al. 2008. Subdiffraction multicolor imaging of the nuclear periphery with 3D structured illumination microscopy. *Science.* 320:1332–1336. https://doi.org/10.1126/science.1156947

Schuh, M., and J. Ellenberg. 2007. Self-organization of MTOCs replaces centrosome function during acentrosomal spindle assembly in live mouse oocytes. *Cell.* 130:484–498. https://doi.org/10.1016/j.cell.2007.06.025

Serçin, Ö., J.-C. Larsimont, A.E. Karambelas, V. Marthiens, V. Moers, B. Boeckx, M. Le Mercier, D. Lambrechts, R. Basto, and C. Blanpain. 2016. Transient PLK4 overexpression accelerates tumorigenesis in p53-deficient epidermis. *Nat. Cell Biol.* 18:100–110. https://doi.org/10.1038/ncb3270

Sinigaglia, C., D. Thiel, A. Hejnol, E. Houliston, and L. Leclère. 2018. A safer, urea-based in situ hybridization method improves detection of gene expression in diverse animal species. *Dev. Biol.* 434:15–23. https://doi.org/10.1016/j.ydbio.2017.11.015

Sonnen, K.F., L. Schermelleh, H. Leonhardt, and E.A. Nigg. 2012. 3D-structured illumination microscopy provides novel insight into architecture of human centrosomes. *Biol. Open.* 1:965–976. https://doi.org/10.1242/bio.20122337

Striano, P., M. Malacarne, S. Cavani, M. Pierluigi, R. Rinaldi, M.L. Cavaliere, M.M. Rinaldi, C. De Bernardo, A. Coppola, M. Pintaudi, et al. 2006. Clinical phenotype and molecular characterization of 6q terminal deletion syndrome: five new cases. *Am. J. Med. Genet. A.* 140:1944–1949. https://doi.org/10.1002/ajmg.a.31435

Terret, M.E., C. Lefebvre, A. Djiane, P. Rassinier, J. Moreau, B. Maro, and M.-H. Verlhac. 2003. DOC1R: a MAP kinase substrate that control microtubule organization of metaphase II mouse oocytes. *Development.* 130:5169–5177. https://doi.org/10.1242/dev.00731

Touati, S.A., and K. Wassmann. 2016. How oocytes try to get it right: spindle checkpoint control in meiosis. *Chromosoma.* 125:321–335. https://doi.org/10.1007/s00412-015-0536-7

Verlhac, M.H., C. Lefebvre, P. Guillaud, P. Rassinier, and B. Maro. 2000. Asymmetric division in mouse oocytes: with or without Mos. *Curr. Biol.* 10:1303–1306. https://doi.org/10.1016/S0960-9822(00)00753-3

Wieczorek, D., M. Krause, F. Majewski, B. Albrecht, D. Horn, O. Riess, and G. Gillessen-Kaesbach. 2000. Effect of the size of the deletion and clinical manifestation in Wolf-Hirschhorn syndrome: analysis of 13 patients with a de novo deletion. *Eur. J. Hum. Genet.* 8:519–526. https://doi.org/10.1038/sj.ejhg.5200498

Zhang, C.-Z., A. Spektor, H. Cornils, J.M. Francis, E.K. Jackson, S. Liu, M. Meyerson, and D. Pellman. 2015. Chromothripsis from DNA damage in micronuclei. *Nature.* 522:179–184. https://doi.org/10.1038/nature14493